Ultrasonic properties of random media under uniaxial loading

M. F. Insana[a)]
Department of Biomedical Engineering, University of California, One Shields Avenue, Davis, California 95616

T. J. Hall
Department of Radiology, University of Kansas Medical Center, 3901 Rainbow Boulevard, Kansas City, Kansas 66160

P. Chaturvedi
Sprint PCS, 15405 College Boulevard, Lenexa, Kansas 66219

Ch. Kargel
Department of Biomedical Engineering, University of California, One Shields Avenue, Davis, California 95616

Acoustic properties of two types of soft tissue-like media were measured as a function of compressive strain. Samples were subjected to uniaxial strains up to 40% along the axis of the transducer beam. Measurements were analyzed to test a common assumption made when using pulse-echo waveforms to track motion in soft tissues—that local properties of wave propagation and scattering are invariant under deformation. Violations of this assumption have implications for elasticity imaging procedures and could provide new opportunities for identifying the sources of backscatter in biological media such as breast parenchyma. We measured speeds of sound, attenuation coefficients, and echo spectra in compressed phantoms containing randomly positioned scatterers either stiffer or softer than the surrounding gelatin. Only the echo spectra of gel media with soft scatterers varied significantly during compression. Centroids of the echo spectra were found to be shifted to higher frequencies in proportion to the applied strain up to 10%, and increased monotonically up to 40% at a rate depending on the scatterer size. Centroid measurements were accurately modeled by assuming incoherent scattering from oblate spheroids with an eccentricity that increases with strain. While spectral shifts can be accurately modeled, recovery of lost echo coherence does not seem possible. Consequently, spectral variance during compression may ultimately limit the amount of strain that can be applied between two data fields in heterogeneous media such as lipid-filled tissues. It also appears to partially explain why strain images often produce greater echo decorrelation in tissues than in commonly used graphite–gelatin test phantoms. © *2001 Acoustical Society of America.* [DOI: 10.1121/1.1414703]

PACS numbers: 43.80.Cs, 43.35.Bf [FD]

I. INTRODUCTION

The theory of acoustic wave propagation in heterogeneous media[1] can successfully explain many aspects of ultrasonic scattering measurements in soft biological tissues when essential material properties are known.[2] Except for blood, we know little about the exact anatomical microstructure that scatters ultrasound. We know that energy is redirected at spatial fluctuations in medium mass density ρ and bulk compressibility κ. Furthermore, compressibility fluctuations $\Delta\kappa = \kappa - \bar{\kappa}$ for collagen and elastin are often substantial[3] with respect to the spatial average $\bar{\kappa}$, whereas the corresponding density fluctuations, e.g., from lipid-filled structures, are less but significant: values for $\bar{\kappa}\Delta\rho/\rho\Delta\kappa$ have been measured in the range of 0 to 0.5 for blood, liver, and skeletal muscle.[4,5]

Coupling this information with mathematical analyses that link scatterer size to ultrasonic frequency spectra,[6,7] investigators have studied the inverse problem of identifying scattering structures[8] and thus are able to track *in vivo* changes in the microvascular diameter below the diffraction limit for diagnostic wavelengths.[9,10] Ultimately, similarities between matched ultrasonic and histological measurements are used to verify the sources of scattering based on size, number density, and collagen content. In this paper we describe another discriminating scattering feature that may be useful in defining scattering sources—changes in the centroid of the backscattered echo spectrum with the amount of applied strain.

The idea for this study originated during early elasticity imaging experiments designed to investigate relationships between large- and small-scale viscoelastic properties of tissue-like media.[11] It is essential that local acoustic properties be invariant under strain if we are to obtain accurate time delay estimates from echo correlation analysis. Specifically, the microscopic spatial distribution of tissue bulk moduli that dominates scattering properties in soft tissues must be uncorrelated with the macroscopic spatial distribution of tissue shear moduli that determines the appearance of strain

---
[a)]Electronic mail: mfinsana@ucdavis.edu
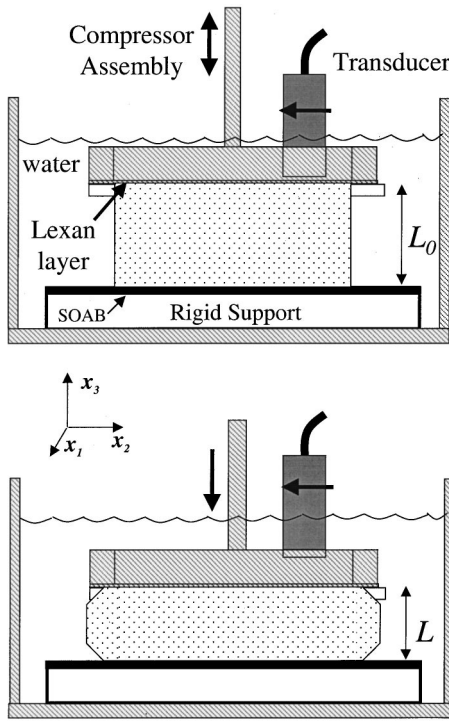
FIG. 1. The apparatus for measuring acoustic properties of cylindrical samples is illustrated (top). The force was applied downward against an immobile Lucite block by the Lexan layer deforming the sample (bottom). The sound-absorbing (SOAB) rubber was included during backscatter measurements and removed during speed and attenuation measurements. The transducer beam axis was oriented normal to and scanned parallel to the Lucite block surface through the Lexan.

images.[12] Only then can echo correlation provide a reliable method for tracking object motion.

In this paper we summarize a series of experiments involving two classes of materials originally developed by Madsen *et al.* as ultrasound phantoms.[13] Type I materials are glass-sphere-in-gelatin suspensions and type II materials are oil-droplet-in-gelatin dispersions. The diameter ranges of glass microspheres in the type I samples are either small (35–75 μm) or large (150–180 μm). All glass microspheres are randomly positioned and much stiffer than the surrounding gelatin. Type II materials contain oil spheres dispersed randomly throughout the gelatin. The mean oil sphere diameter varies in different samples between 20 and 400 μm. At room temperature, the oils are liquids, similar to the lipid at body temperature, and therefore much softer than the surrounding gelatin.

We measured speeds of sound, attenuation coefficients, and backscattered echo spectra for each sample up to 10 MHz and for applied uniaxial stresses producing strains up to 0.4. Samples were compressed in a plane normal to the top planar surface such that all points on the surface were displaced the same amount along $-x_3$ (Fig. 1). No attempt was made to match the acoustic properties of the gel samples to specific body tissues. Instead, we sought to produce samples with sound speed, attenuation, and backscatter features within the range of values reported for human soft tissues.[14] The results below indicate the reliability of echo tracking in a broad range of deformations for tissue-like media, and sug-

TABLE I. Type I materials: Glass-in-gel suspensions.

Sample	Glass sphere diameter (μm)	Mass (g/l)	Sound speed at 2.5 MHz (m/s)	Atten. coefficient (dB/cm) at 2.5/5.0/7.5/10.0 MHz
1	35–75	33.3	1590	0.74/1.88/3.83/6.91
2	150–180	6.67	1575	0.47/1.10/1.67/2.71

gest a new method for identifying the anatomical sources of bioacoustic scattering.

II. MATERIALS AND METHODS

Type I Materials.[15] One-hundred twenty grams of animal hide gelatin (type A, 275 bloom, Fisher Scientific, Hampton, NH) were mixed into each liter of a 6% *n*-propanol-in-water solution at room temperature. The mixture was placed in a 29 mm Hg vacuum for a few minutes to remove gases. The beaker of dissolved, degassed gelatin was then heated at 45 °C in a water bath for about 90 min until it became translucent. The clear gelatin solution was removed from the heat, glass microspheres (Potters Industries, Inc., Valley Forge, PA) as specified in Table I were added and thoroughly mixed with a spoon, and the beaker was cooled to 30 °C while stirring. The liquid glass–gel mixture was poured into a cylindrical mold 7.5 cm in diameter and 2.5 cm in height, sealed, and rotated at 1 rpm overnight. Congealed samples were removed from the molds and stored at room temperature in a sealed container with a small amount of propanol–water solution to minimize desiccation. Samples 1 and 2 in Table I are type I. Samples A and B (see Sec. III) are also type I, but have no added scatterers.

Type II Materials.[13] More of the clear gelatin solution described above was heated in a water bath to 70 °C. Instead of glass microspheres, 250 ml of an oil were emulsified into each liter of liquid gelatin by vigorous mixing with a spoon. The different types of oils used in this study are listed in Table II. Care was taken to prevent introducing air while mixing. The emulsion was cooled to 30 °C before being poured into the cylindrical molds and rotated in room air overnight. After congealing and removal from its mold, an inspection microscope was used to measure the average di-

TABLE II. [a]Type II Materials: Oil[b]-in-gel dispersions.[c]

Sample	Oil type	Oil conc. (ml/l)	Sound speed (m/s) at 2.5 MHz	Atten. coefficient (dB/cm) at 2.5/5.0/7.5/10.0 MHz
3	corn	250	1557	1.18/3.69/6.90/10.78
4	motor	250	1556	0.87/3.68/7.56/11.79
5	peanut	250	1561	0.95/3.72/6.85/10.65
6	mineral	250	1567	0.87/2.86/5.03/7.47

[a]The acoustic properties listed in Tables I and II are for uncompressed samples. Averaging attenuation coefficients for samples 3–5 gives the following least-squares fit to a second-order polynomial between 0 and 10.0 MHz, where we include $\alpha(0)=0$ dB/cm: $\alpha_{3-5}(f)=-0.1253+0.3700f+0.0760f^2$. The fits for samples 1 and 2 yield, respectively, $\alpha_1(f)=-0.0034+0.0659f+0.0619f^2$, and $\alpha_2(f)=-0.1407+0.1925f+0.0087f^2$.
[b]The motor oil was SAE 10W30.
[c]Data from two corn-oil samples were obtained. The two samples are referred to as sample 3 and sample 3′ in the figures.

Insana *et al.*: Ultrasonic properties of random media

ameter of oil drops visible from the surface of the colloid, now a dispersion. Samples 3–6 in Table II are type II.

Strain. In the following, we report an engineering strain $\epsilon' = (L_0 - L)/L_0$ as that resulting from the compressive stress applied.[16] L_0 is the initial sample height along the compression axis, x_3 in Fig. 1, and L is the instantaneous height. If the stiffness of the sample is uniform throughout its volume, then ϵ' approximates the spatial derivative of displacement along x_3, i.e., $\epsilon' \simeq \partial u_3 / \partial x_3$.

Strain for the finite displacements used in this study is defined in the Lagrangian frame as[17]

$$\epsilon_{33} = \frac{\partial u_3}{\partial x_3} + \frac{1}{2}\left[\left(\frac{\partial u_1}{\partial x_3}\right)^2 + \left(\frac{\partial u_2}{\partial x_3}\right)^2 + \left(\frac{\partial u_3}{\partial x_3}\right)^2\right]. \quad (1)$$

ϵ_{33} is the Lagrangian strain tensor that describes deformation of a unit volume along the x_3 axis. If the derivatives are small, then $\epsilon_{33} \simeq \partial u_3 / \partial x_3$, the infinitesimal strain tensor, which is approximately ϵ' for homogeneous media. $\partial u_3 / \partial x_3$ is not small in this study. Nevertheless, we use ϵ' to specify the strain for convenience. Readers can convert between Lagrangian and engineering strains using $\epsilon_{33} \simeq \epsilon'(1 + \epsilon'/2)$.

Measurement geometry has a large influence on steady-state deformation patterns in stressed samples, often more than material properties such as elastic modulus and Poisson's ratio ν. For these nearly incompressible media, parallel-plate compressor geometry, full-slip boundary conditions, and quasistatic measurement conditions, sample volume is conserved. We treat samples under these conditions as Hookean elastic solids,[17] so that $\epsilon_{11} = \epsilon_{22} = -\nu\epsilon_{33}$.

Acoustic measurements. Measurements were made in distilled/degassed water at room temperature (between 18.8 and 20.4±1 °C) with the apparatus diagrammed in Fig. 1. The transducers had one circular PZT element, 19 mm in diameter, that was focused at f/2.8 (videoscan immersion, Panametric, Waltham, MA). Two transducers with nominal frequencies 3 and 10 MHz were used in this study. Test samples were deformed by uniformly displacing the top surface of the sample downward a known amount ±4 μm. Applied forces were held several minutes before recording waveforms to minimize variability caused by viscous creep. With the possible exception of the mineral oil sample, each test sample contained a sufficient number of scatterers per resolution volume (>5–10) to be considered an incoherent scattering source.

A pulse-echo variation on the narrow-band-through-transmission substitution technique described by Madsen *et al.*[13] was used to measure sound speed and attenuation. Sinusoidal pressure bursts were transmitted through the sample and reflected at normal incidence at the surface of a 5-cm-thick Lucite block. The sound-absorbing (SOAB) layer shown in Fig. 1 was removed. The duration of the voltage burst that excited the transducer was adjusted between 10 and 20 cycles to avoid reverberations. The transducer–reflector distance remained unchanged during the experiment and was approximately equal to the radius of curvature of the spherically focused transducers. The compressive force was applied to the sample through a 1-mm thick Lexan layer that was rigidly attached to the compressor assembly. This layer

may have flexed slightly during compression; a 1-mm flexure at $\epsilon' = 0.4$ corresponds to a -10% strain error for 25-mm-thick samples.

We recorded measurements of echo phase ϕ and amplitude A near the center of the voltage burst as viewed from a digital oscilloscope display. The phase was estimated from the time shift in a zero crossing near the center of the burst. $M = 10$ independent measurement pairs (A_m, ϕ_m), $1 \leq m \leq M$, were obtained after scanning the transducer at 2-mm lateral increments with the sample in place. Only five phase measurements were used to estimate sound speed while all ten were used to estimate attenuation. One reference measurement pair (A_0, ϕ_0) was recorded with the sample removed. Wave properties in the latter case are determined entirely by the distilled water, but, in both situations, the thin Lexan layer used to compress the sample remained in place.

The substitution technique involves an expression for the speed of sound in a sample, $c(\epsilon', T)$ (m/s), as a function of ϵ', measurement temperature T (°C), speed of sound in water[18] $c_0(T)$ (m/s), sample thickness $d(\epsilon')$ (m), and mean temporal phase shift introduced by placing the sample in the sound beam $\Delta\phi$ (s) $= (\Sigma_{m=1}^{M} \phi_m)/M - \phi_0$. Writing $\Delta\phi(\epsilon', T) = 2d(\epsilon')[1/c(\epsilon', T) - 1/c_0(T)]$ and rearranging terms, we find

$$c(\epsilon', T) = \frac{2d(\epsilon')c_0(T)}{2d(\epsilon') + c_0(T)\Delta\phi(\epsilon', T)}. \quad (2)$$

Attenuation coefficients, $\alpha(f, \epsilon', T)$, at frequency f (MHz) were found from the ratio of peak-to-peak burst amplitudes with $[A = (\Sigma_{m=1}^{M} A_m)/M]$ and without (A_0) the sample in place and sample thickness d via

$$\alpha(f, \epsilon', T) = \frac{10}{d(\epsilon')} \log_{10} \frac{A(f, \epsilon', T)}{A_0(f, T)}. \quad (3)$$

Castor oil was used as a standard sample to calibrate attenuation estimates.[13] Large-amplitude sinusoids were transmitted, yet the amplitude was not so large as to violate linearity and agreement ($\pm 3\%$) with published values for attenuation in castor oil: $0.834f^{5/3}$ (dB/cm) at 20 °C.[19]

Following measurements of sound speed and attenuation, echo spectra were recorded. We digitized 10.24 μs echo time series generated by the backscatter of broadband pulses within a sample. The transmitted pulse duration was approximately two cycles, producing a -6-dB bandwidth of 60% of the peak frequency for pulses reflected from a Lucite surface in water at 20 °C. A Panametrics (Waltham, MA) pulser–receiver Model 5052UA was used. M was increased to 25 waveforms, each digitized at 8 bits and 5×10^7 samples/s to give $N = 512$ points per waveform. Adjusting the transducer–sample distance, we placed the center of the time series at the radius of curvature of the transducer. A SOAB layer was used as shown in Fig. 1 to reduce reverberations.

The magnitude of the discrete Fourier transform $|G[k]|$, $0 \leq k \leq N/2 - 1$, was computed using a fast Fourier transform algorithm.[20] From the set of recorded time series, $g_{m\epsilon}[n]$, $0 \leq n \leq N - 1$, at each strain value ϵ', we estimated the mean frequency spectrum,
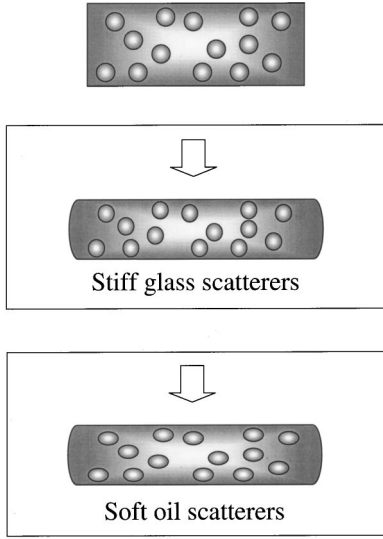
FIG. 2. An illustration of sample deformation. Stiff scatterers redistribute but do not deform during uniaxial compression. Soft spherical scatterers redistribute and deform into oblate spheroids during deformation. Scatterers are not to scale.

$$|G_\epsilon[k]| = \frac{1}{M} \sum_{m=1}^{M} \left| \sum_{n=0}^{N-1} g_{m\epsilon}[n] e^{-i2\pi kn/N} \right|. \qquad (4)$$

The summation over M waveforms yields an approximation to an ensemble average.[21]

Echo spectra shown in Sec. III below describe a shift in the peak value of $|G_\epsilon[k]|$ with increasing ϵ'. We summarized changes in echo spectra by a scalar value obtained from estimates of the normalized first moment or spectral *centroid*,[22]

$$f_c(\epsilon') = \Delta f \frac{\sum_{k=0}^{N/2} k |G_\epsilon[k]|}{\sum_{k=0}^{N/2} |G_\epsilon[k]|}, \qquad \Delta f = \frac{1}{NT}, \qquad (5)$$

where T is the sampling interval, in this case 20 ns. The centroid indicates any monotonic weighting of spectral values, such as those expected for a change in the scattering function with ϵ'.

Statistical analysis. We state our confidence that acoustic parameters vary as a function of engineering strain ϵ' using the following analysis. The mean $\bar{y}$ and variance $\hat{\sigma}_y^2$ are sample moments of the (assumed) normally distributed parameter y, and are computed from M uncorrelated measurements. The expected value, $E\{y\}$, will fall within the interval[23]

$$\bar{y} - \frac{\hat{\sigma}_y t_{M-1;\gamma/2}}{\sqrt{M}} \leqslant E\{y\} \leqslant \bar{y} + \frac{\hat{\sigma}_y t_{M-1;\gamma/2}}{\sqrt{M}}, \qquad (6)$$

with $100(1-\gamma)$ percent confidence. Setting $\gamma = 0.01$, we find the 99% confidence interval. Values found outside of this interval are assumed to be from a different distribution. We used look-up tables[23] and experimental parameters to find the threshold value $t_{M-1;\gamma/2}$ that determines the probability $\Pr(t_{M-1} > t_{M-1;\gamma/2}) = \int_{t_{M-1;\gamma/2}}^{\infty} p(t) dt = \gamma/2$. t_{M-1} is the student t statistic; $t_{9;0.005} = 3.250$ and $t_{4;0.005} = 4.604$.

Intersample attenuation coefficients varied widely. Consequently, we normalized $\alpha(\epsilon')$ values relative to that at $\epsilon' = 0$ to find $\beta(\epsilon') = \alpha(\epsilon')/\alpha_0$ for studying ϵ' dependences.

Assuming the attenuation estimates at different values of ϵ' are independent and that the variance σ_α^2 is independent of ϵ', then the uncertainty in β is found by propagating errors according to[24]

$$\sigma_\beta = \left[\sigma_\alpha^2 \left(\frac{\partial \beta}{\partial \alpha} \right)^2 + \sigma_{\alpha_0}^2 \left(\frac{\partial \beta}{\partial \alpha_0} \right)^2 \right]^{1/2} = \frac{\sigma_\alpha}{\alpha_0} \sqrt{1 + \beta^2}. \qquad (7)$$

The error bars in Fig 4 are examples of σ_β.

Centroid predictions. It is reasonable to assume that soft scatterers in compressed samples will deform in the manner of the surrounding gelatin (Fig. 2). Changes in the ultrasonic echo spectrum may be predicted if we understand how the backscatter spectrum from oblate spherical oil droplets varies with eccentricity. Oils in type II samples are approximately spherical with radius r_0 before compression. After deformation into oblate spheroids, the minor axis will be $r_1 = (1 - \epsilon') r_0$ for $0 \leqslant \epsilon' < 1$. To conserve volume, the major axis must therefore be $r_2 = r_0 / \sqrt{(1-\epsilon')}$, so the eccentricity is $\sqrt{1 - (r_1/r_2)^2} = \sqrt{1 - (1-\epsilon')^3}$. Fortunately expressions that describe scattering from an acoustically soft oblate spheroid are available. See Appendix A for details.

We computed scatter fields from one oblate spheroid insonated with many plane waves at frequencies in the transducer bandwidth. Assuming that only incident waves are scattered (single-scatter Born approximation[1]) and that the scatter field at the receiving aperture is entirely incoherent, we integrated the exact numerical solution for the pressure field at frequency f, i.e., $p_f(\mathbf{x}, t, \epsilon')$ from Appendix A. The integration is over the transducer aperture to find the net force at the surface.[25] The net force was multiplied by a Gaussian pulse-echo system response, $H(f)$ (Appendix B), computed for the same frequencies, and then integrated over frequency to give the echo signal samples $\tilde{g}_\epsilon[n]$. Taking the discrete Fourier transform and finding the magnitude, we arrive at the predicted echo spectrum, $|\tilde{G}_\epsilon[k]|$. Finally, the predicted spectral centroid, $\tilde{f}_c(\epsilon')$, was computed from Eq. (5), where $|\tilde{G}_\epsilon[k]|$ replaced $|G_\epsilon[k]|$.

III. RESULTS

Sound speed. Figure 3 shows that the speed of sound does not vary significantly over the range $0 \leqslant \epsilon' \leqslant 0.2$ for three oil-in-gel dispersion samples, all having scatterers more compressible than the background gelatin. Invariance was determined by finding that all the measurement points for a given sample fall within the 99% confidence interval (± 6.9 m/s) about the mean value for that sample. Including data from type I media with stiff scatterers (not shown in Fig. 3), we determined the speeds of sound in each sample tested were independent of the applied strain, i.e., $c(\epsilon', T) = c(T)$.

Attenuation. Figure 4 shows the relative change in the attenuation coefficient for samples when $\epsilon' \leqslant 0.2$. There is a slight increase with compression, e.g., the linear regression analysis gives $\beta(\epsilon') = \alpha(\epsilon')/\alpha_0 = 0.76\epsilon' + 0.993$ at 2.5 MHz and $\beta(\epsilon') = 0.25\epsilon' + 0.991$ at 5.0 MHz. There is no physical reason for assuming a linear dependence, so these equations are just a convenience. One point at 2.5 MHz and one at 5 MHz fall outside the 99% confidence interval for stating that the expected value for β is one.
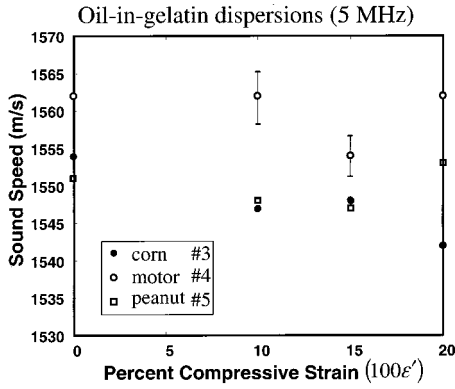
FIG. 3. Speeds of sound are plotted as a function of percent compression for oil-in-gel dispersions: ●, sample 3; ○, sample 4; and □, sample 5. Sample numbers are listed in Tables I and II. Error bars indicate ±one standard deviation.

The apparent increases in β with ϵ' in Fig. 4 could result from the changing geometry of the experiment rather than material properties of the sample. Because sound speeds are significantly higher in all samples ($1556 \, \text{m/s} \leqslant c \leqslant 1590 \, \text{m/s}$) than in the surrounding water ($1483 \, \text{m/s}$), it is possible that compression varies the degree of sound wave refraction and thus modifies the echo detected. We explored this possibility by constructing samples A and B. Both are type I materials and neither contained added scatterers. The only difference is
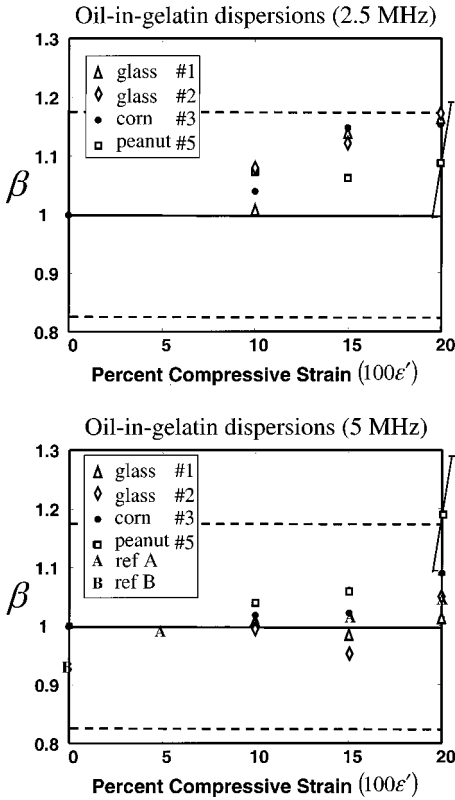
FIG. 4. Attenuation coefficients in dB/cm, normalized by the values at 0% compression, $\beta(\epsilon') = \alpha(\epsilon')/\alpha_0$, are plotted versus percent compression. (a) 2.5 MHz and (b) 5.0 MHz. △, sample 1; ◇, sample 2; ●, sample 3; and □, sample 5. Error bars indicate $\pm \sigma_\beta$. In (b), points labeled A and B refer to measurements on samples A and B, as discussed in Sec. III. The solid line is $\beta(\epsilon') = 1$ and the dashed lines define the 99% confidence interval that the expected value is unity.
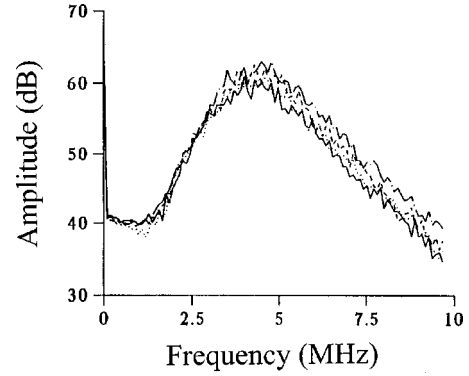
FIG. 5. Backscattered echo spectra via Eq. (4) are plotted for sample 3 at 0% (solid), 10% (dotted), 20% (dashed), and 30% (dot–dashed) compression.

that sample A is 2.5 cm thick while sample B is 2.0 cm thick (80% of A). We also eliminated the thin Lexan compression layer from the measurement and replaced it with a 2.5-cm thick agar plate having a speed of sound matched to distilled water at room temperature to avoid reverberation. The elastic modulus of the agar was approximately 500 times that of the gelatin sample and therefore did not deform significantly during sample compression.

The attenuation coefficients, Eq. (3), for uncompressed samples A and B at 5 MHz are α_A (5 MHz, 0, 22 °C)=0.69 ±0.12 dB/cm and α_B (5 MHz, 0, 22 °C)=0.64±0.16 dB/cm. $\beta(\epsilon')$ increases slightly with ϵ' for sample A, similar to the type I samples with scatterers [Fig. 4(b)], reaching a maximum at $\beta(0.2)=1.043$. The experimental conditions for sample A compressed to $\epsilon'=0.2$ and uncompressed sample B are identical, so the 7% attenuation difference, if significant, can only be due to the stress in sample A. The difference is not significant, however, because the lack of scatterers reduces the attenuation value and hence increases the relative uncertainty: $\beta_{B/A}(0)=\alpha_B(0)/\alpha_A(0)=0.928\pm0.262$ (s.d.).

We conclude (a) that it is the varying measurement geometry and/or an absorption process in the stressed gelatin that produces a small increase in attenuation with ϵ', the former being most likely. (b) Surface reverberations and the magnitude of volumetric scattering do not affect β. (c) There is no significant difference in β for type I and II samples. Consequently, we set $\alpha(f,\epsilon',T) \simeq \alpha(f,T)$ for the purpose of spectral estimation. This decision is discussed further in Sec. III and Appendix B.

Backscatter. Figure 5 suggests an obvious change in the backscatter echo spectra with ϵ' for the corn oil sample. As this sample is compressed, the amplitudes of high-frequency spectral components are increased more than those at lower frequencies. This trend is more clearly visible in the measured centroid shifts plotted in Fig. 6; $\Delta f_c = f_c(\epsilon') - \bar{f}_c(0)$, where $\bar{f}_c(0)$ is the average value for all six uncompressed samples listed in Tables I and II. Note that $f_c(0)$ is determined primarily by the response of the ultrasound system for random scattering media, so it is not surprising that the centroids measured for each undeformed sample are similar. For $0 \leqslant \epsilon' \leqslant 0.3$, the centroid shifts measured for the two glass-in-gel samples were essentially zero. That is expected for stiff scatterers that are spatially reoriented but not individually
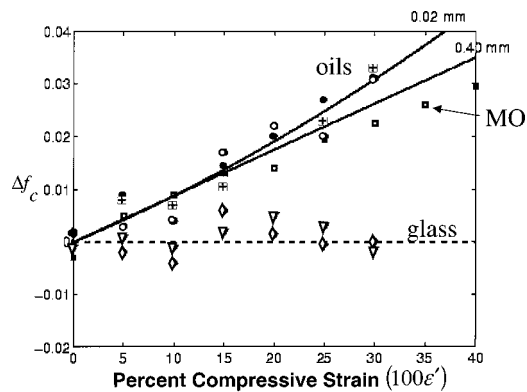
FIG. 6. Measured change in centroid values for stiff scatterers ($\diamond$, sample 1 and $\triangledown$, sample 2) and soft scatterers ($\bullet$, sample 3; $+$, sample 3′; $\bigcirc$, sample 5; and $\square$, sample 6). Measured values obtained via Eq. (5) were subtracted from the average value of all samples measured at 0% compression. Data from the mineral oil sample is marked MO. Solid curves are predicted centroid shifts for oil-droplet spheroidal scatterers with uncompressed diameters of 20 and 400 μm.

deformed—the scattering function is unchanged. The number density of scatterers remains constant with ϵ' because the gelatin volume is conserved under deformation. However, liquid oil scatterers, being softer than the gel, easily deform with the gelatin, which alters the scattering function. Since the centroid frequency increases, it appears that the change in oil drop shape results in increased scattering at higher frequencies.

Measured values of Δf_c for oil-in-gel samples are plotted as points along with predicted values, $\Delta \tilde{f}_c$, displayed as solid lines in Fig. 6. We see larger centroid shifts for smaller oil drops at higher compressions. We examined the surface of several oil-in-gel samples under an inspection microscope and found that the two corn oil and the peanut oil samples had the smallest mean oil-drop diameter, roughly 20 μm. The average diameter of mineral oil drops was much larger, roughly 400 μm. The oil-drop size appears to be determined by oil viscosity and mixing time. The agreement among measured and predicted values in Fig. 6 leads us to conclude that the deformation of scatterers softer than the background produces measurable and predictable changes in the *mean* echo spectrum not observed with scatterers much stiffer than the background.

Samples were found to fracture at $0.3 < \epsilon' < 0.4$. Therefore c, α measurements were limited to $\epsilon' < 0.2$ to ensure sample integrity for scattering measurements. Echo spectra were acquired on each sample at 5% increments until fractures became evident.

IV. DISCUSSION

Scattering in most soft biological tissues is believed to be a small percentage of the total attenuation. Absorption mechanisms dominate propagational losses.[26] Based on more than a decade of experimentation with phantoms, our impressions are that scattering equals or exceeds absorptive losses in glass-in-gel samples with glass-sphere diameters greater than 20 μm, and absorption dominates attenuation in the oil-in-gel dispersion samples. However, measurements of total scattering cross sections are needed to make that determi-

nation, and those measurements have not been made. Given these observations, it is not surprising that the mean echo spectrum in compressed dispersions can change without significantly affecting attenuation. We did not correct the spectral estimates for the slight increase in attenuation with ϵ'. Had we applied the correction, the centroid shift Δf_c would be slightly larger and the difference between type I and II scatterers in Fig. 6 would be greater. Also, correcting echo spectra for $\beta(\epsilon')$ would yield an in increase Δf_c for type I materials, which seems likely. These effects are examined quantitatively in Appendix B.

The observed spectral variance suggests that echo waveforms from lipid-filled biological media, such as breast tissue, can decorrelate when strained. Figure 6 shows that Δf_c is proportional to ϵ' for compressions up to 10%. Greater than 10%, the magnitude of the centroid shift depends on scatterer diameter, increasing faster for smaller Rayleigh scatterers than larger Mie scatterers. This source of waveform decorrelation, which has not been discussed in the literature previously, could pose fundamental limitations for elasticity imaging of tissues with lipid-filled scattering sites.

We anticipated the effects of simple scaling strains on the frequency response of scattering from random *point* targets, and suggested a pulse-shaping method to mitigate waveform decorrelation.[11] Pulse shaping would be helpful for strain estimation in the glass-in-gel samples. However, the deformation of finite-size scatterers, as described in this report, further decorrelates echo waveforms in a manner that cannot be anticipated or compensated in an individual spectrum, e.g., that from a single time series. Scatterer deformation changes the scattering response and hence is an irreversible source of echo decorrelation. Strain imaging algorithms that work well in simulation or using phantom data, usually perform at a reduced level in tissues, in the sense that decorrelation noise is increased.[27]

Spectral variance poses problems for strain imaging but also offers opportunities to identify the sources of scattering in biological media. Measurements of Δf_c in breast tissues, for example, may be used to distinguish the relative contribution of scattering from collagen-filled (stiff) versus lipid-filled (soft) structures. If $\Delta f_c = 0$, we can assume any lipid component to the tissue acts as a matrix media that contains scatterers but does not scatter sound significantly. Alternatively, if the centroid increases linearly with compression, then it is likely that soft, deformable scatterers play a significant role in echo formation.

V. CONCLUSIONS

The average sound speed, attenuation, and echo spectrum from random, tissue-like scattering media containing stiff spheres is unchanged by uniaxial compressions up to 40%. This finding verifies a fundamental assumption required for strain imaging using these media. However, the mean echo spectrum increases with compressive strain preferentially at high frequency and in a predictable manner for media containing deformable scatterers. Consequently, the use of ultrasonic echoes to track movement of lipid-filled scattering objects in the body will suffer additional waveform decorrelation in proportion to ϵ'. These effects were

observed in phantoms but have yet to be examined in biological tissues. Our results suggest caution in designing strain imaging techniques and new opportunities for identifying scattering sources in biological media.

ACKNOWLEDGMENTS

APPENDIX A

In this appendix we briefly summarize the scattering equation for the oblate spheroid described by Senior and Uslenghi,[28] which is applied in the last part of Sec. II.

An oblate spheroid is formed by rotating an ellipse about its minor axis. Plane sound waves at wavelength λ and temporal frequency f,

$$p_i = \exp[i2\pi(x_3/\lambda - ft)], \tag{A1}$$

are assumed to be incident on the spheroid. The minor spheroid axis, direction of wave propagation, and direction of the applied deformation force are all oriented along x_3 (Fig. 1). The time-independent form of the scattered pressure in the farfield of one acoustically soft spheroid ("soft" means the pressure difference across the scatterer surface is zero) is

$$p_f = -2\sum_{n=0}^{\infty} \frac{i^n}{N_n(-iq)} \frac{R_n^{(1)}(-iq, i\xi_1)}{R_n^{(3)}(-iq, i\xi_1)}$$
$$\times R_n^{(3)}(-iq, i\xi_1) S_n(-iq, -1) S_n(-iq, \eta). \tag{A2}$$

(ξ, η, ϕ) are spheroidal coordinates related to rectangular coordinates (x_1, x_2, x_3) via

$$x_1 = \frac{b}{2}\sqrt{(\xi^2+1)(1-\eta^2)}\cos\phi,$$
$$\tag{A3}$$
$$x_2 = \frac{b}{2}\sqrt{(\xi^2+1)(1-\eta^2)}\sin\phi, \quad x_3 = \frac{b}{2}\xi\eta,$$

where $0 \leq \xi < \infty$, $-1 \leq \eta \leq 1$, and $0 \leq \phi < 2\pi$. ξ and η contours form sets of confocal ellipses and hyperbolas, respectively, that have been rotated about the minor axis, which is parallel to x_3. The surface $|\xi| = \xi_1$ (constant) defines the scatterer boundary with major axis length $b(\xi^2+1) = r_0/\sqrt{1-\epsilon'}$ and minor axis length $b|\xi| = (1-\epsilon')r_0$. The last two expressions give the relationship between engineering strain and scatterer geometry in elliptical coordinates. q is the product of the wave number, $2\pi/\lambda$, and half the elliptical interfocal distance, $b/2$.

The advantage of elliptical coordinates is that the wave equation becomes separable in terms of radial and angular solutions. $R_n^{(j)}(-ic', i\xi)$, $j = 1,2,3$ are radial spheroidal wave functions of the jth kind, and $S_n(-ic', \eta)$ are angular spheroidal wave functions, where n is a positive integer. [Note that plane waves incident along the minor axis means that the subscript integer m found for these wave functions in (Ref. 28) is zero. For example, $R_{mn}^{(j)}(-ic', i\xi)|_{m=0} \equiv R_n^{(j)}(-ic', i\xi)$.] These are the radial and angular "solutions" to

the wave equation in spheroidal coordinates. $S_n(-ic', \eta)$ are found from expansions in associated Legendre functions of the first kind.[29] Similarly, $R_n^{(j)}(-ic', i\xi)$ are formed from sums of weighed spherical Bessel functions. $N_n(-ic')$ are functions of associated constants, including eigenvalues for the differential equation. These are formed using recurrence formulas and tables of constants given by Flammer.[29] The notation, derivations, and formulas coded in FORTRAN and MATLAB for our application are due to Flammer, although relations described by Lowan in Chap. 21 of Abramowitz and Stegun on spherical wavefunctions[30] were helpful. Readers wishing to do the same should be aware of differences in the coordinate systems used in these[28–31] and other references and a few typos, e.g., a missing minus sign in Eq. (3.1.7) in Ref. 29.

Tabulated values for functions and constants are given in several of the references cited above. These were used to determine the number of terms in the respective sums needed for convergence. Convergence was established when the computed values varied from the tabulated values less than 0.01%.

APPENDIX B

In this appendix we explore the magnitude of the effects of ultrasonic frequency-dependent attenuation on the spectral centroid and explains our model for echo formation.

Assume a linear, time-invariant imaging system that maps the acoustic impedance function for the object being scanned, $z(x)$ into an echo sample g_m via the convolution integral adapted from Maurice and Bertrand,[32]

$$g_m = \left[\int_{-\infty}^{\infty} dx\, h\left(t_m - \frac{2x}{c}\right) z''(x)\right] + n_m.$$

Acoustic impedance and its second derivative, $z'' = \partial^2 z/\partial x^2$, are generally functions of three spatial dimensions but for this purpose are simplified to one dimension x. Derivatives are taken along the direction of wave travel. n_m is a noise sample. $h(t)$ is the pulse-echo impulse response, having carrier frequency f_0 and pulse-length parameter σ_t, that we model for all time t assuming the Gaussian form,

$$h(t) = \frac{1}{\sqrt{2\pi}\sigma_t}\exp(-t^2/2\sigma_t^2)\sin(2\pi f_0 t). \tag{B1}$$

It is known that if you represent the object function $z(x)$ as a spatially uncorrelated Gaussian random variable, the expected frequency spectrum of the echo data is determined by the impulse response of the imaging system.[33] Furthermore, it has been shown that the echo amplitude from a Gaussian pulse undergoing Rayleigh scattering and exponential attenuation remains Gaussian, although the peak frequency and spectral width vary (see Appendix C in Ref. 34). Consequently, it is reasonable to represent the magnitude of the echo frequency response as

$$|H(f)| = \exp[-2\pi^2(f-f_0)^2\sigma_t^2], \quad f \geq 0 \tag{B2}$$

where $H(f)$ is the Fourier transform of $h(t)$. From Eq. (5), it can be shown that the centroid frequency for $|H(f)|$ is f_0.

Our concern is the change in spectral centroid from excess attenuation caused by sample compression. We model the effects of excess attenuation as a change in the frequency response of the measurement system,

$$|H(f,\epsilon')| = \exp[-2\pi^2(f-f_0)^2\sigma_t^2]$$
$$\times \exp[-\mathcal{A}(f,\epsilon')], \quad f \geq 0. \tag{B3}$$

The excess attenuation, $\mathcal{A}(f,\epsilon')$, is found from the ratio of attenuation factors,

$$\exp[-\mathcal{A}(f,\epsilon')] = \frac{\exp[-2(\alpha L - \alpha_0 L_0)]}{\exp[-2\alpha_0(L-L_0)]}$$
$$= \exp[-2L(\alpha-\alpha_0)],$$

where $\alpha \equiv \alpha(f,\epsilon') \geq \alpha_0 \equiv \alpha(f,0)$, and L_0, L are the sample thicknesses before and after compression producing strain ϵ'. Therefore

$$\mathcal{A}(f,\epsilon') = 2L(\alpha-\alpha_0) = 2\alpha_0 L_0(1-\epsilon')(\beta-1), \tag{B4}$$

where $\beta = \alpha/\alpha_0$ and $\epsilon' = (L_0-L)/L_0$ were defined previously. If there is no excess attenuation, $\alpha = \alpha_0$ and $\mathcal{A}(f,\epsilon') = 0$.

We modeled the attenuation coefficient in Eq. (B4) as a quadratic function of frequency, $\alpha_0 = q_0 + q_1 f + q_2 f^2$; see Tables I and II. Defining the constants $C = 2L_0(1-\epsilon')(\beta-1)$, $C_1 = 1 + q_2 C/2\pi^2\sigma^2$, and combining the exponent of Eq. (B3) with Eq. (B4) and the quadratic attenuation model, we find

$$-2\pi^2\sigma_t^2\left(f^2 - 2ff_0 + f_0^2 + C\frac{q_0+q_1f+q_2f^2}{2\pi^2\sigma_t^2}\right)$$
$$= -2\pi^2\sigma_t^2 C_1\left[f^2 - \frac{2}{C_1}\left(f_0 - \frac{Cq_1}{4\pi^2\sigma^2}\right)f + \frac{f_0^2}{C_1}\right.$$
$$\left. + \frac{Cq_0}{2\pi^2\sigma^2 C_1}\right]. \tag{B5}$$

Adding and subtracting the term

$$\frac{1}{C_1^2}\left(f_0 - \frac{Cq_1}{4\pi^2\sigma^2}\right)^2$$

from Eq. (B5) allows us to complete the square and find

$$-2\pi^2\sigma_t^2 C_1\left\{\left[f - \frac{1}{C_1}\left(f_0 - \frac{Cq_1}{4\pi^2\sigma^2}\right)\right]^2 - \frac{f_0^2}{C_1^2}(1-C_1)\right\}$$
$$+ \frac{C^2 q_1^2}{8\pi^2\sigma_t^2 C_1^2} - \left(Cq_0 + \frac{f_0 q_1 C}{C_1}\right). \tag{B6}$$

The effect of excess attenuation $\mathcal{A}(\epsilon') > 0$ on the magnitude of the backscattered spectrum is given by terms that depend on frequency, viz., the first term in Eq. (B6). The spectral width is modified by the factor C_1 and the centroid is downshifted from f_0 by the amount

$$\frac{1}{C_1}\left(f_0 - \frac{Cq_1}{4\pi^2\sigma_t^2}\right) - f_0. \tag{B7}$$

Figure 4(a) shows $\beta_{max} \simeq 1.17$ at $\epsilon' = 0.2$. In all cases $L_0 = 2.54$ cm. The coefficients q_0, q_1, and q_2 for the samples

are listed in Tables I and II (in dB). For a Gaussian pulse at 2.5 MHz center frequency having a full-width-at-half-maximum value of two wavelengths, $\sigma_t = 1/\sqrt{2\ln 2}f_0 = 0.34 \mu$s. With these values and Eq. (B7), the attenuation-compensated centroid shifts measured for the oil-in-gel samples would increase values in Fig. 6, at most, by 13 kHz at $\epsilon' = 0.2$. Corresponding values of Δf_c for the glass-in-gel samples would increase, at most, 6.5 kHz for sample 1 and 4.1 kHz for sample 2 if compensated for attenuation. Thus compensating for attenuation effects on the backscatter spectra would increase the relative differences between the measurements for type I and II samples shown in Fig. 6.

[1] A. Ishimaru, *Wave Propagation and Scattering in Random Media: Single Scattering and Transport Theory* (Academic, New York, 1978), Vol. I.

[2] R. C. Waag, IEEE Trans. Biomed. Eng. **31**, 884 (1984).

[3] S. Fields and F. Dunn, J. Acoust. Soc. Am. **54**, 809 (1973).

[4] D. K. Nassiri and C. R. Hill, J. Acoust. Soc. Am. **79**, 2048 (1986).

[5] R. C. Waag, D. Dalecki, and P. E. Christopher, J. Acoust. Soc. Am. **85**, 423 (1989).

[6] F. Lizzi, M. Ostromogilsky, E. Feleppa, M. Rorke, and M. Yaremko, IEEE Trans. Ultrason. Ferroelectr. Freq. Control **34**, 319 (1987).

[7] M. F. Insana and D. G. Brown, "Acoustic scattering theory applied to soft biological tissues," in *Ultrasonic Scattering in Biological Tissues*, edited by K. K. Shung and G. A. Thieme (CRC Press, Boca Raton, 1993), pp. 75–124.

[8] J. H. Rose, M. R. Kaufman, S. A. Wickline, C. S. Hall, and J. G. Miller, J. Acoust. Soc. Am. **97**, 656 (1995).

[9] D. J. Coleman, *et al.*, Eur. J. Ophthalmol. **5**, 96 (1995).

[10] M. F. Insana, J. G. Wood, T. J. Hall, G. G. Cox, and L. A. Harrison, Ultrasound Med. Biol. **21**, 1143 (1995).

[11] M. Bilgen and M. F. Insana, J. Acoust. Soc. Am. **99**, 3212 (1996).

[12] The bulk modulus $\mathcal{K}$ is traditionally defined from the pressure/volume ratio and describes how a medium changes volume when subjected to a force (Ref. 35). The shear modulus $\mathcal{G}$ is traditionally defined from the shear stress/shear strain ratio and describes how a medium changes shape when subjected to a force. In soft biological tissues $\mathcal{K} \gg \mathcal{G}$ so that the elastic modulus $= 9\mathcal{G}\mathcal{K}/(3\mathcal{K}+\mathcal{G}) \simeq 3\mathcal{G}$ and Poisson's ratio $= 3\mathcal{K}-2\mathcal{G}/(6\mathcal{K}+2\mathcal{G}) \simeq 0.5$.

[13] E. L. Madsen, J. A. Zagzebski, and G. R. Frank, Ultrasound Med. Biol. **8**, 277 (1982).

[14] S. Goss, R. Johnston, and F. Dunn, J. Acoust. Soc. Am. **68**, 93 (1980).

[15] T. J. Hall, M. Bilgen, M. F. Insana, and T. A. Krouskop, IEEE Trans. Ultrason. Ferroelectr. Freq. Control **44**, 1355 (1997).

[16] Engineering strain is often defined as the negative of this quantity. Since we are most interested in compressive deformations, it is convenient to drop the minus sign.

[17] Y. C. Fung, *A First Course in Continuum Mechanics*, 3rd ed. (Prentice–Hall, Englewood Cliffs, NJ, 1994).

[18] M. Greenspan and C. E. Tschiegg, J. Acoust. Soc. Am. **31**, 75 (1959).

[19] F. Dunn, P. D. Edmonds, and W. J. Fry, "Absorption and dispersion of ultrasound in biological media," in *Biological Engineering* (McGraw-Hill, New York, 1969), pp. 214–215.

[20] A. V. Oppenheim, R. W. Schafer, and J. R. Buck, *Discrete-Time Signal Processing*, 2nd ed. (Prentice–Hall, Upper Saddle River, NJ, 1999).

[21] To avoid confusion, we note here that spectral estimates for single-trace time series do vary with compression. In fact, those changes have been used to estimate blood velocity (Ref. 36) and strain (Ref. 37). An ensemble average of time series yields an echo spectrum that depends only on the scattering and absorption coefficients of the random medium and the system response function. Because the system response does not change, variations in the average echo spectrum with compression are caused by changes in the medium properties.

[22] R. N. Bracewell, *The Fourier Transform and Its Applications*, 2nd ed. (McGraw-Hill, New York, 1978).

[23] J. Bendat and A. Piersol, *Random Data Analysis and Measurement Procedures*, 2nd ed. (Wiley, New York, 1986).

[24] P. R. Bevington, *Data Reduction and Error Analysis for the Physical Sciences* (McGraw-Hill, New York, 1969).

[25] M. F. Insana, R. F. Wagner, D. G. Brown, and T. J. Hall, J. Acoust. Soc. Am. **87**, 179 (1990).

3250   J. Acoust. Soc. Am., Vol. 110, No. 6, December 2001

Insana *et al.*: Ultrasonic properties of random media

[26] M. E. Lyons and K. J. Parker, IEEE Trans. Ultrason. Ferroelectr. Freq. Control **35**, 511 (1988).

[27] Y. Zhu, P. Chaturvedi, and M. F. Insana, Ultrason. Imaging **21**, 127 (1999).

[28] J. J. Bowman, T. B. A. Senior, and P. L. E. Uslenghi, *Electromagnetic and Acoustic Scattering by Simple Shapes* (North-Holland, Amsterdam, 1969), Chap. 13.

[29] C. Flammer, *Spheroidal Wave Functions* (Stanford University Press, Stanford, CA, 1957).

[30] A. N. Lowan, ''Spheroidal wave functions,'' in *Handbook of Mathematical Functions With Formulas, Graphs, and Mathematical Tables*, edited by M. Abramowitz and I. Stegun (Dover, New York, 1965).

[31] P. M. Morse and H. Feshbach, *Methods of Theoretical Physics* (McGraw-Hill, New York, 1953).

[32] R. L. Maurice and M. Bertrand, IEEE Trans. Med. Imaging **18**, 593 (1999).

[33] R. F. Wagner, S. W. Smith, J. M. Sandrick, and H. Lopez, IEEE Trans. Sonics Ultrason. **30**, 156 (1983).

[34] M. F. Insana, L. T. Cook, M. Bilgen, and P. Chaturvedi, J. Acoust. Soc. Am. **107**, 1421 (2000).

[35] N. W. Tschoegl, *The Phenomenological Theory of Linear Viscoelastic Behavior* (Springer-Verlag, Heidelberg, 1989).

[36] J. A. Jensen, *Estimation of Blood Velocities Using Ultrasound* (Cambridge University Press, New York, 1996).

[37] E. E. Konofagou, T. Varghese, J. Ophir, and S. K. Alam, Ultrasound Med. Biol. **25**, 1115 (1999).